nature communications

Article

https://doi.org/10.1038/s41467-024-54392-x

Arsenic-induced enhancement of diazotrophic recruitment and nitrogen fixation in *Pteris vittata* rhizosphere

Received: 29 January 2024

Accepted: 7 November 2024

Published online: 19 November 2024

Check for updates

Jiahui Lin[1,2], Hengyi Dai[1,2], Jing Yuan[3], Caixian Tang[4], Bin Ma[1,2] & Jianming Xu[1,2]

Heavy metal contamination poses an escalating global challenge to soil ecosystems, with hyperaccumulators playing a crucial role in environmental remediation and resource recovery. The enrichment of diazotrophs and resulting nitrogen accumulation promoted hyperaccumulator growth and facilitated phytoremediation. Nonetheless, the regulatory mechanism of hyperaccumulator biological nitrogen fixation has remained elusive. Here, we report the mechanism by which arsenic regulates biological nitrogen fixation in the arsenic-hyperaccumulator *Pteris vittata*. Field investigations and greenhouse experiments, based on multi-omics approaches, reveal that elevated arsenic stress induces an enrichment of key diazotrophs, enhances plant nitrogen acquisition, and thus improves plant growth. Metabolomic analysis and microfluidic experiments further demonstrate that the upregulation of specific root metabolites plays a crucial role in recruiting key diazotrophic bacteria. These findings highlight the pivotal role of nitrogen-acquisition mechanisms in the arsenic hyperaccumulation of *Pteris vittata*, and provide valuable insights into the plant stress resistance.

Ferns, with a lineage extending back 400 million years, have undergone extensive evolutionary processes shaped by natural selection, resulting in a diverse array of forms and species adapted to various environments[1]. Ma et al. (2001) documented a brake fern known as *Pteris vittata*, capable of adapting to and accumulating excessive arsenic (As) from As-contaminated soils[2], positioning it as an promising candidate for As phytoremediation. The unique growth characteristics of *Pteris vittata* allow it to thrive in As concentrations that could be lethal to other plants[3]. However, our current understanding of the mechanisms behind this phenomenon is limited.

Nitrogen (N) is a critical element in regulating microbial and plant growth, thereby influencing the effectiveness of phytoremediation[4,5]. Diazotroph-mediated biological N fixation presents a promising strategy to enhance phytoremediation of heavy metal-contaminated soils. In detail, diazotrophs utilize the nitrogenase to convert atmospheric N_2 into ammonia[6], increasing N availability to plant roots and thereby supporting the development of sufficient biomass necessary for effective phytoremediation. Previous studies observed the important roles of diazotrophs in phytoremediation. For instance, diazotrophic bacteria (e.g. *Rhizobium* spp. and *Pseudomonas* spp.) support the growth of the heavy metal-tolerant plant *Miscanthus sinensis* by enhancing biological N fixation[7]. Diazotrophs from Alphaproteobacteria, Deltaproteobacteria, and Cyanobacteria are notably enriched in the rhizosphere of *Pteris vittata* in mining areas, facilitating heavy metal accumulation in the plant[8]. Intercropping hyperaccumulators, such as *Pteris vittata*[9], *Sedum alfredii*[10] and *Odontarrhena chalcidica*[11], with legumes can enhance phytoextraction by leveraging efficient legume diazotrophic microbiome. Despite the recognized importance

[1]Institute of Soil and Water Resources and Environmental Science, College of Environmental and Resource Sciences, Zhejiang University, Hangzhou, China. [2]Zhejiang Provincial Key Laboratory of Agricultural Resources and Environment, Zhejiang University, Hangzhou, China. [3]Department of Environmental Science and Forestry, Connecticut Agricultural Experiment Station, New Haven, CT, USA. [4]La Trobe Institute for Sustainable Agriculture and Food, Department of Animal, Plant & Soil Sciences, Bundoora, VIC, Australia. e-mail: jmxu@zju.edu.cn

of N in phytoremediation, the mechanisms by which hyperaccumulator plants regulate biological N fixation remain elusive.

Arsenic oxidation is mediated by both heterotrophic and chemoautotrophic microorganisms[12]. Arsenic-dependent N fixation is reported in various As-associated environments; For instance, *Serratia* species utilize As oxidation as an alternative electron donor for chemolithotrophic N fixation in tailings[13]. In the plant rhizosphere, abundant carbon sources provide a favorable environment for heterotrophic microbiota[14], selectively enriching functional microorganisms that drive processes like organic compound degradation and N fixation[15]. In As-rich habitats, resistant plants can rid root cells of toxic metalloids through a detoxification strategy that involves the efflux of arsenite[16]. This rhizosphere process provides substrates for As oxidation while inhibiting arsenite-intolerant species, potentially expanding the niche for heterotrophic As-oxidized diazotrophs. Despite the widely observed enrichment of *aioA* and *nifH* genes in the rhizosphere of *Pteris vittata*[8,17,18], the interplay between As oxidation and heterotrophic N fixation remains inadequately understood.

Plant roots are naturally exposed to diverse abiotic stresses and respond by exuding a variety of metabolites which modulate the assembly dynamics of root-associated microbiome to mitigate the encountered stress[19]. Flavonoids have been considered crucial root-released signal molecules mediating the interaction of roots with microbes[20–23]. For instance, apigenin and luteolin were produced by maize under N deprivation, which promoted the enrichment of the *Oxalobacteraceae* bacteria in the rhizosphere, leading to enhanced plant growth and N acquisition by stimulating root proliferation[24]. Naringenin, produced by *Arabidopsis*, induced chemotaxis in *Aeromonas* sp. H1 to enhance plant dehydration resistance by increasing H_2O_2 accumulation in guard cells and promoting stomatal closure, alongside upregulating jasmonic acid-related regulators[25]. Beneficial microbes associated with hyperaccumulators can enhance phytoremediation efficiency by transforming heavy metal(loid)s, increasing the bioavailability of nutrients and minerals, activating plant stress response systems, and promoting the production of growth-stimulating hormones[26]. For example, Rhizobiales[17] and Burkholderiales[18], identified as key As oxidizers in the root-associated habitats of *Pteris vittata*, are instrumental in improving phytoremediation. Notably, a recent study reported that As stress significantly enhanced the biosynthesis of flavonoids in *Pteris vittata*[27], suggesting a potential role in modulating the rhizosphere microbiome.

In this study, we explore the regulatory mechanism of biological N fixation in As-hyperaccumulator *Pteris vittata* based on a comprehensive research framework (Supplementary Fig. 1). The field survey and greenhouse experiment revealed that As stress enhanced biological N fixation in the rhizosphere. Metagenomic analysis based on *nifH*-Palmscan (an identification approach based on catalytic motifs) taxonomically recognized As-upregulated diazotrophic taxa. Isolation and greenhouse experiments further demonstrated the N fixation, As oxidation, and plant growth promotion abilities of key diazotrophic bacteria (e.g. *Bradyrhizobium* sp. J3 and *Rhizobium* sp. G5). Furthermore, multidimensional metabolomics identified As-upregulated rhizosphere metabolites, with their chemoattractant effects on these beneficial diazotrophs validated via the In-Situ Chemotaxis Assay (ISCA) platform. Our findings shed light on a mechanism by which increased As stress can promote the release of the flavonoid catechin from *Pteris vittata* roots, thereby facilitating the recruitment of key diazotrophic bacteria, such as *Rhizobium* sp. G5 and *Bradyrhizobium* sp. J3. Concurrently, arsenite efflux from the roots may support the establishment of diazotrophic communities and enhance the N-fixation potential of heterotrophic As-oxidizing diazotrophs (e.g., *Rhizobium* sp. G5). Collectively, these processes enhance N availability through enhancing biological N fixation in the rhizosphere, supporting plant growth and boosting the efficiency of phytoremediation.

Results

Arsenic promotes nitrogen fixation in the rhizosphere

To investigate the impact of As on N dynamics in the field, the concentrations of four N indices, total N, dissolved total N, ammonium-N (NH_4^+) and nitrate-N (NO_3^-), were determined in both rhizosphere and bulk soils. Irrespective of As stress level, N indices were significantly higher in the rhizosphere than in the bulk soil ($P = 0.0006$, two-sided Wilcoxon tests). Interestingly, the elevation in As stress significantly enhanced the four N indices in the rhizosphere soil but not bulk soils, except for a slight increase in NO_3^-. The paired comparisons between rhizospheric and bulk soils also highlighted a robust increase in N accumulation in the rhizosphere under high-As stress (Fig. 1a). Furthermore, three As indices (As(V), As(III) and total As) positively correlated with four N indices (Supplementary Fig. 2). These results suggest that elevated As stress promoted the cycling and accumulation of N in the rhizosphere of *Pteris vitatta*.

Principal Coordinate Analysis (PCoA) and Analysis of Similarity (ANOSIM) showed that the bacterial communities in the rhizosphere significantly differed from those in the bulk soil (Supplementary Fig. 3; ANOSIM: $R = 0.25$; $P = 0.0002$). Additionally, the correlation coefficients between the PC1, PC2 and PC3 and As indices show a notable increase compared with those of the corresponding bulk soil, highlighting a robust correlation between microbial community and As in the rhizosphere (Fig. 1b and Supplementary Table 1). These consistent findings were also evident in a broader investigation of rhizosphere bacterial communities in *Pteris vitatta*, affirming the general impact of As stress on the assembly of rhizosphere bacterial communities (Supplementary Fig. 4). Furthermore, 314 *nifH*, 1624 *nifD* and 1949 *nifK* homologs were gathered from metagenomic assembled open reading frames (ORFs) obtained from 25 rhizosphere metagenomic samples. Quantitative analysis indicated that the abundances of *nifH*, *nifD*, and *nifK* homologs in the rhizosphere were significantly higher under the high-As stress than low-As stress, and were positively correlated with the As indices (Fig. 1c and Supplementary Fig. 5). This implies that elevated As stress enhances the N-fixing potential in the rhizosphere.

To confirm the heightened N input in the rhizosphere induced by elevated As, a greenhouse pot experiment using in-situ soil was performed (soil details are available in Supplementary Table 2). The experiment comprised three soil treatments for plant cultivation (control, As(V) amendment, and NH_4^+ amendment) along with corresponding bulk soils without plants. After two months of growth, the plants in the NH_4^+-treated group exhibited a 4-fold increase in biomass production compared with the control group, indicating N deficiency in the control group. Meanwhile, a 63% increase in biomass and increases in total N concentration in both roots and shoots under As stress compared with control group, suggest the potential role of As in alleviating N limitations (Fig. 1d, e). The results of qPCR showed a significant increase in the *nifH* abundance in rhizosphere soils compared with bulk soils. Notably, As addition elevated the abundance of *nifH* in the rhizosphere by 91% (Fig. 1f). All these indicate the important role of As in both N accumulation and diazotroph enrichment in the rhizosphere.

Identification of diazotrophs with *nifH*-Palmscan

To precisely identify *nifH* from the homologs, a *nifH* scanner, *nifH*-Palmscan, was developed based on the framework of Palmscan[28] and model the palmprint of the nifH protein—a segment of the sub-domain with well-conserved catalytic motifs (Fig. 2a). Further details regarding the training and validation of *nifH*-Palmscan are available in the Supplementary Information.

Thirty one *nifH* representative sequences were identified from the rhizosphere using the *nifH*-Palmscan to scrutinize *nifH* homologs, followed by a 95% amino acid clustering. The quantification of these *nifH* groups remained consistent with previous observations (Supplementary Fig. 6). Phylogenetic analysis was conduct on these *nifH* groups and a database consisted of 1268 validated *nifH* variants with

https://doi.org/10.1038/s41467-024-54392-x

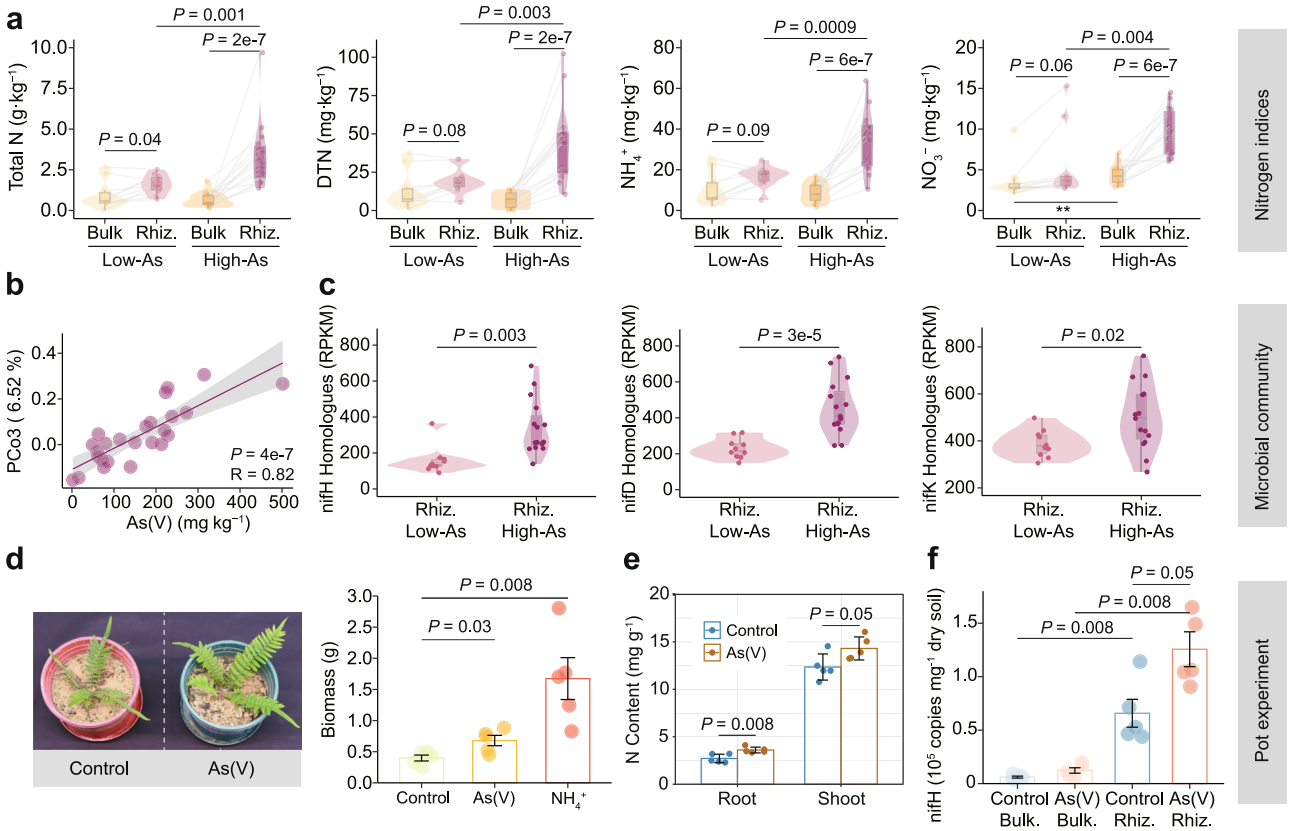

Fig. 1 | Arsenic stress promotes biological nitrogen fixation in *Pteris vittata*, alleviating nitrogen limitation for plant growth. a Differences in N indices including total N, dissolved total N (DTN), NH_4^+ and NO_3^-, across the bulk (Bulk) and rhizosphere (Rhiz.) soils under low- ($n = 10$ for each habitat) and high-As stresses ($n = 15$ for each habitat). **b** Correlation between beta-diversity patterns of rhizospheric bacterial communities and As(V) concentration. **c** Variations of *nifH*, *nifD*, and *nifK* homologs in the rhizosphere between the low- ($n = 10$) and high-As stresses ($n = 15$). **d** Photograph portraying *Pteris vittata* cultivated for 50 days under the control and As(V) addition, along with the aboveground dry weight of plants under control, As(V) and N amendment. **e** Comparison of the total N content of root and shoot between the control and As treatments. **f** Variations in the abundance of *nifH* across the bulk and rhizosphere soils under the control and As treatments based on qPCR quantification. In box plots, the center line represents the median, box edges delimit lower and upper quartiles and whiskers show the highest and lowest values. For (**d**–**f**), data are shown as mean ± SEM ($n = 5$). Each data point represents a biologically independent replicate. *P* values were determined through two-sided Wilcoxon test.

taxonomic labels. The results revealed that all *nifH* sequences fell into 8 distinct nitrogenase groups (Fig. 2b). Of these, 71% originated from Proteobacteria and 16% were from Desulfobacterota. Notably, 61% of *nifH* representative sequences were associated with Rhizobiales and Burkholderles. Differential analysis showed that high-As stress increased the abundances of 65% of the *nifH* representatives, encompassing genera such as *Bradyrhizobium*, *Rhizobium*, *Methyloceanibacter*, *Ideonella*, *Sulfuricella*, *Leptothrix*, *Paraburkholderia*, *Cupriavidus*, *Pseudomonas*, *Azonexus*, *Anaeromyxobacter*, *Geobacter*, and *Propionispora*. Significantly, four *nifH* representatives from the genera *Bradyrhizobium*, *Rhizobium*, *Leptothrix*, and *Cupriavidus* exhibited notable upregulation, identifying them as As-upregulated diazotrophic genera.

Taxonomic annotation of genes associated with As metabolism was conducted based on metagenomic assembled ORFs, revealing distinct patterns of diversity and distribution. The gene *aioA* (encoding the large subunit of As(III) oxidase) exhibited a relatively low diversity and was mainly present in the Rhizobiales and Burkholderiales orders, with a relatively high annotation proportion at the phylum (96%), class (94%), and order (78%) levels (Fig. 3a). In contrast, other genes related to As metabolism, such as *arsC* (associated with As reduction) and *arsM* (associated with As methylation), displayed a broader taxonomic spectrum, spanning across 18 and 23 phyla, respectively. Nevertheless, their annotation coverage was lower, reaching only 52% and 77%, even at the phylum level (Supplementary Fig. 7).

Besides, the differential analysis of ASVs highlighted that those bacterial taxa from Rhizobiales and Burkholderiales exhibited the most substantial upregulation in response to heightened As stress (Supplementary Fig. 8a). When extending our investigations to larger-scale *Pteris vittata* rhizosphere communities, a consistent enrichment of bacteria from Rhizobiales and Burkholderiales was observed in the rhizosphere samples from all four sites, in contrast to the corresponding bulk soils (Supplementary Fig. 8b). These results emphasize the significance of these two taxa in microbial community assembly of *Pteris vittata*.

Rhizospheric diazotrophs enhance arsenic oxidation and plant growth

To further validate the As oxidation and plant growth-promoting capabilities of diazotrophs, a total of 47 bacterial strains were isolated from the rhizosphere of *Pteris vittata* under high-As stress. Given the significance of Rhizobiales and Burkholderiales, seven representative isolates from different genera within these two orders were selected for further experiments based on their optimal intra-generic growth rate in N-free medium (Supplementary Fig. 9). Among them, isolates *Bradyrhizobium* sp. J3, *Rhizobium* sp. G5 and *Cupriavidus* sp. N2 phylogenetically overlapped with three of the As-upregulated diazotrophic genera identified by the *nifH*-Palmscan, accounting for 0.5%, 0.2%, and 0.05‰ of the microbiome in the isolated habitats, respectively.

The cultivation experiments with As(III) addition revealed that five genera possessed As(III) oxidation capabilities. The

https://doi.org/10.1038/s41467-024-54392-x

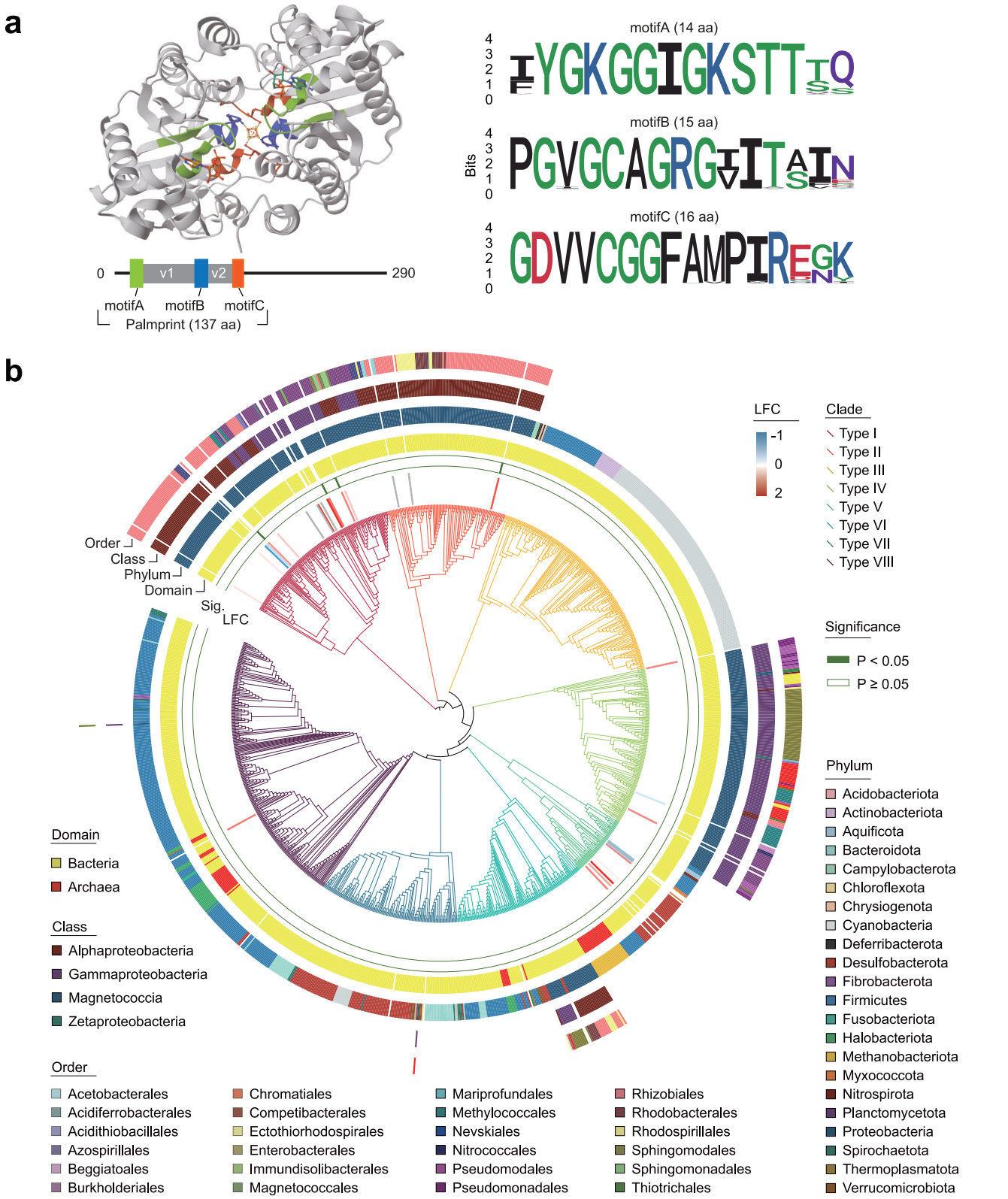

Fig. 2 | Identification of diazotrophs regulated by arsenic stress. a The *nifH* palmprint spans three well-conserved sequence motifs (A, B and C) and intervening variable regions (V1 and V2), exemplified within the *Azotobacter vinelandii* nifH structure (Protein Data Bank code: 6Q93). Conservation was determined by analyzing *nifH* alignments from RefSeq, GeneBank, and NR databases, and depicted using motif sequence logos. aa, amino acids. **b** Maximum-likelihood phylogenetic tree of *nifH* representatives identified from metagenomic assemblies and a custom *nifH* database. The *nifH* sequences, categorized into canonical groups I to VIII, are depicted by branches of varying colors. The innermost circle represents $\log_2$ fold changes (LFC) for up-regulated (red) and down-regulated (blue) *nifH* genes under high As stress versus low As stress. Green labels highlight branches with significant changes (two-sided Wilcoxon tests, adjusted using the Benjamini-Hochberg method). The remaining circles depict the taxonomic annotation of *nifH* at domain, phylum, class, and order levels.

https://doi.org/10.1038/s41467-024-54392-x

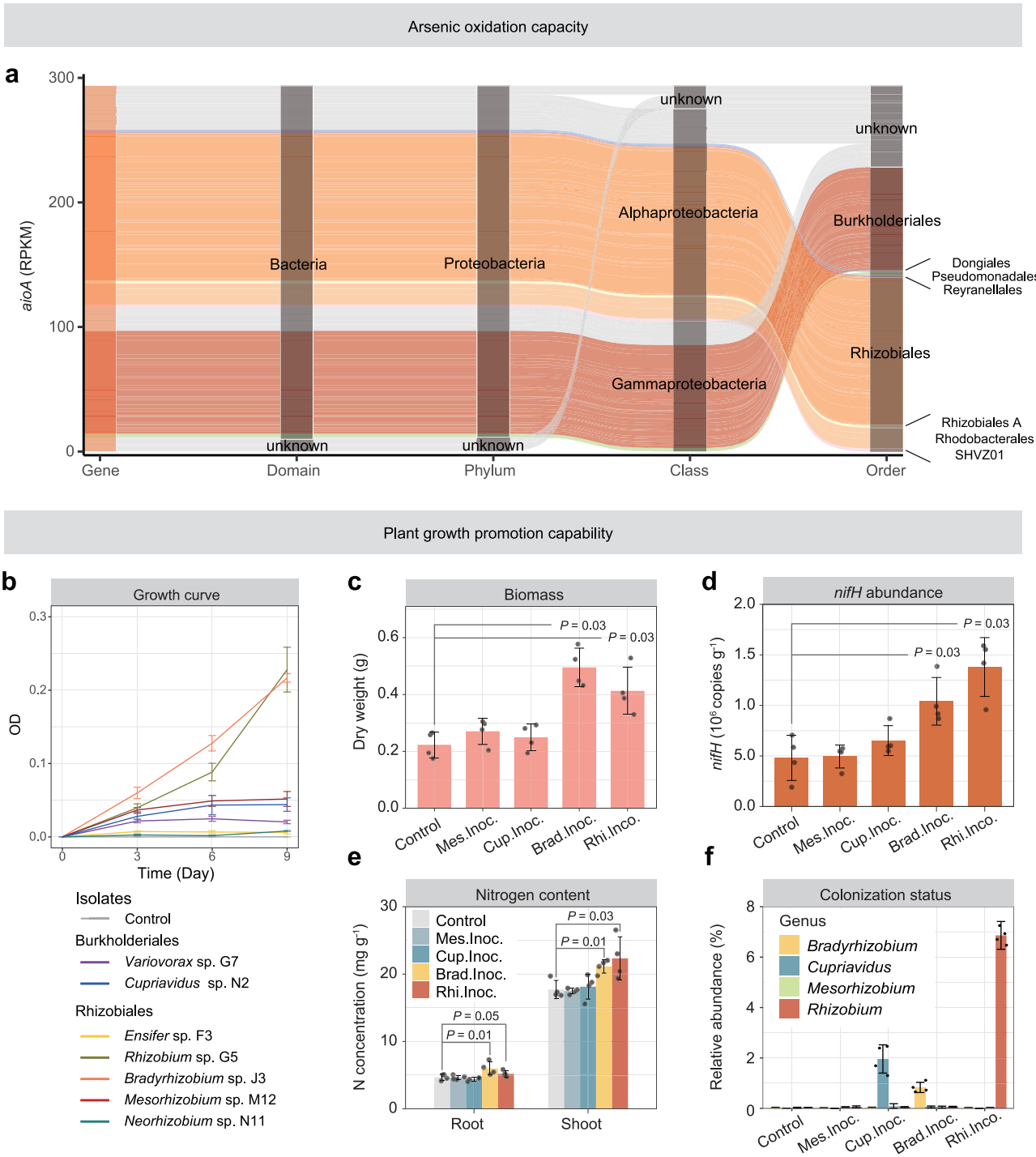

Fig. 3 | Isolation, identification, and functional validation of diazotrophic bacteria. a Sankey plot showing the taxonomy of *aioA* carriers at the domain, phylum, class and order levels. **b** Changes of optical density (OD) in N-free medium amend with As(III) over time after inoculation with seven isolates from seven different genera of Rhizobiales or Burkholderiales ($n = 3$). **c** Effects of isolates inoculation on plant biomass. **d** Effects of isolates inoculation on plant rhizosphere *nifH* abundance. **e** Effects of isolates inoculation on N concentration of root and shoot. **f** Effects of treatments on the relative abundances of *Bradyrhizobium*, *Cupriavidus*, *Mesorhizobium* and *Rhizobium* in the rhizosphere using amplicon. For (**b**–**f**) data are shown as mean ± SEM ($n = 4$). Each data point represents a biologically independent replicate. *P* values were determined through two-sided Wilcoxon tests for each treatment compared to the control group.

Bradyrhizobium sp. J3, *Cupriavidus* sp. N2, *Mesorhizobium* sp. M12, and *Ensifer* sp. F3 demonstrated As(III) oxidation under the N-rich medium (Supplementary Fig. 10a), while *Cupriavidus* sp. N2, *Rhizobium* sp. G5, and *Bradyrhizobium* sp. J3 exhibited As(III) oxidation under the N-free medium (Supplementary Fig. 10b). This demonstrates the presence of As(III) oxidation capabilities across genera within the orders of Rhizobiales and Burkholderiales. Notably, *Bradyrhizobium* sp. J3 and *Rhizobium* sp. G5 displayed superior growth and As(III) oxidation capability in the N-free medium. The acetylene reduction assays, and enzyme-linked immunosorbent assays further confirmed the nitrogenase activity of these two isolates (Supplementary Table 3 and 4).

Subsequently, an inoculation experiment was conducted with *Bradyrhizobium* sp. J3 and *Rhizobium* sp. G5, along with two other

https://doi.org/10.1038/s41467-024-54392-x

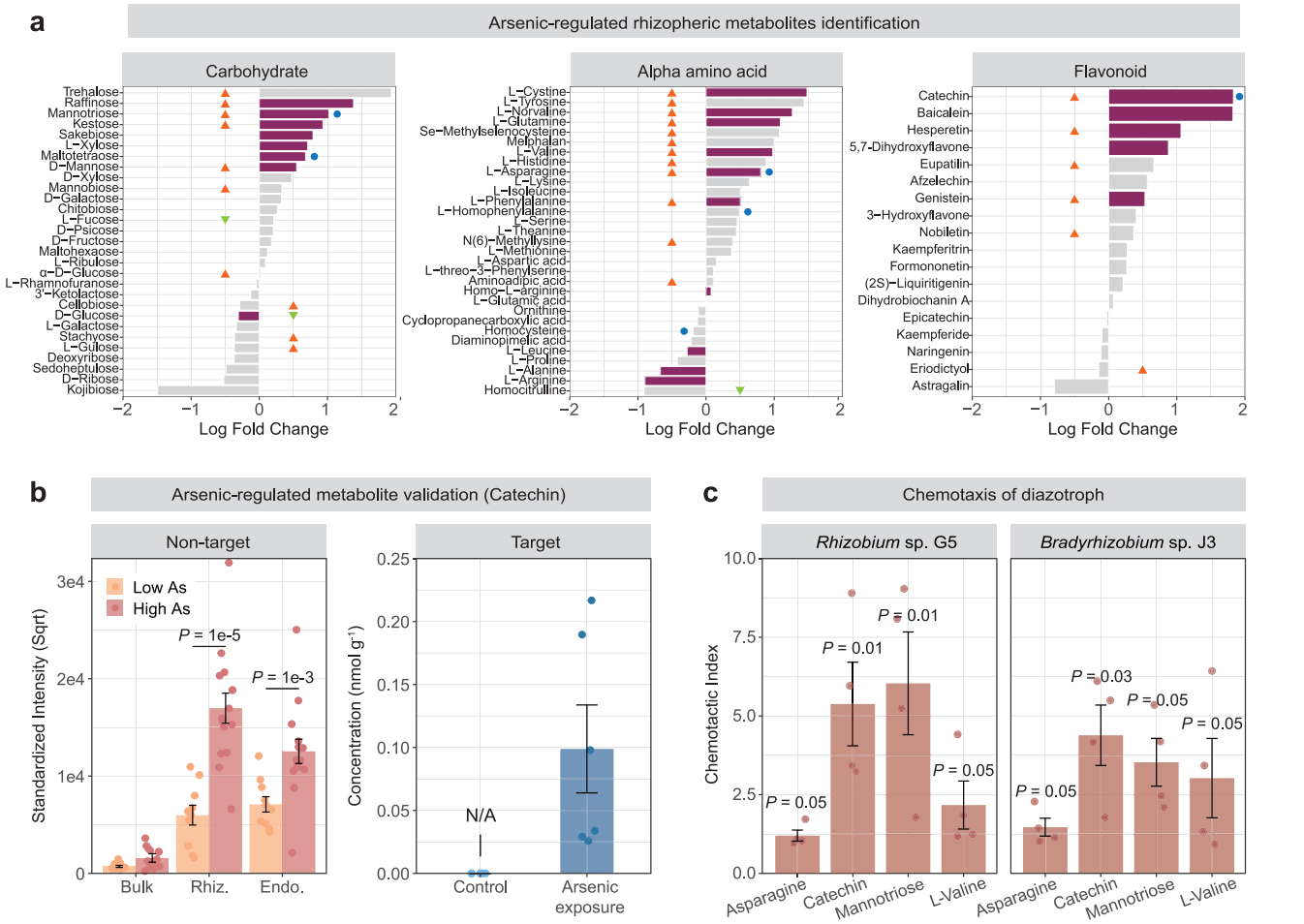

Fig. 4 | Identification of key root exudates regulated by arsenic and their chemotactic effects on diazotrophic isolates. a Bar plots representing the log fold changes in the abundances of carbohydrates, alpha amino acids and flavonoids in the rhizosphere between the low- and high-As stresses. The purple-colored bars represent significant differences while the orange and green triangles, respectively, mark the significantly enriched and depleted metabolites in the high-As rhizosphere compared to the corresponding bulk soil. Blue solid circles indicate up-regulated metabolites in the endosphere under the high-As stress compared with the low-As counterparts. **b** Normalized signal intensity of catechin in the soil-root habitats of wild *Pteris vittata*, including bulk soil, rhizosphere (Rhiz.), and endosphere (Endo.), under low- ($n = 10$ for each habitat) and high-As stresses ($n = 15$ for each habitat), assessed using untargeted metabolomics, and the concentration of catechin in the rhizosphere soil of *Pteris vittata* with and without As exposure in greenhouse experiments, determined using targeted metabolomics ($n = 6$). N/A indicate that the metabolite concentration in the soil was below 5×10^{-3} nmol g^{-1}. *P* values were determined through two-sided Wilcoxon tests. **c** Chemotaxis index of *Rhizobium* sp. G5 and *Bradyrhizobium* sp. J3 exposed to four key metabolites based on In-Situ Chemotaxis Assay (ISCA) microfluidic platform. Chemotaxis index denotes the concentration of cells in ISCA wells containing each metabolite, normalized by the concentration of cells in corresponding wells containing phosphate-buffered saline (PBS). Each metabolite treatment was biologically replicated across four independent ISCA chips ($n = 4$). *P* values between the metabolite treatments and PBS control are determined through one-sided Wilcoxon tests. For (**b**, **c**) data are shown as mean ± SEM.

isolates (*Cupriavidus* sp. N2 and *Mesorhizobium* sp. M12) for comparison. The results indicate that the inoculation with *Bradyrhizobium* sp. J3 and *Rhizobium* sp. G5 significantly increased the shoot weights (Fig. 3c and Supplementary Fig. 11), and the N concentration in both root and shoot tissues (Fig. 3e). Amplicon of 16S rRNA V3-V4 region and qPCR of the *nifH* gene in the rhizosphere confirmed the successful colonization of these two diazotrophs (Fig. 4df).

Interestingly, *Rhizobium* sp. G5 exhibited a rapid growth and significant As(III) oxidation activity in the N-free medium. Furthermore, acetylene reduction assays revealed that the supplementation of As(III) markedly enhanced the N-fixing activity of *Rhizobium* sp. G5 (Supplementary Table 4).

Chemoattractant effects of arsenic-regulated rhizospheric metabolites on diazotrophs

Arsenic stress profoundly impacted the root exudates of *Pteris vitatta*. Overall, the concentration of dissolved organic C in the rhizosphere increased 1.8-fold under the high-As stress compared to low-As stress, while there was no significant difference in bulk soils (Supplementary Fig. 12a). Metabolite profiling revealed distinct separation of bulk soil from the rhizosphere and endosphere along PC1, while PC2 distinguished the endosphere from both the rhizosphere and bulk soils, highlighting the pronounced influence of root exudates on the rhizosphere soil. The ANOSIM test showed that the high-As stress markedly differentiated the composition of metabolites in the rhizosphere (positive ion mode: $P = 0.001$, negative ion mode: $P = 0.001$) and endosphere (positive ion mode: $P = 0.002$, negative ion mode: $P = 0.008$) from those under the low-As stress, highlighting the impact of As on root exudates (Supplementary Fig. 12b).

To elucidate the link between root metabolites and diazotrophs, a comprehensive profiling identified 968 differential metabolites across bulk soil, rhizosphere, and endosphere. Given the critical role of carbohydrates, amino acids, and flavonoids in the chemotaxis of diazotrophs, the analysis highlighted 29 carbohydrates, 31 amino acids, and 18 flavonoids as pivotal metabolic categories for further investigation (Supplementary Data 1). Five criteria were formulated to identify As-

https://doi.org/10.1038/s41467-024-54392-x

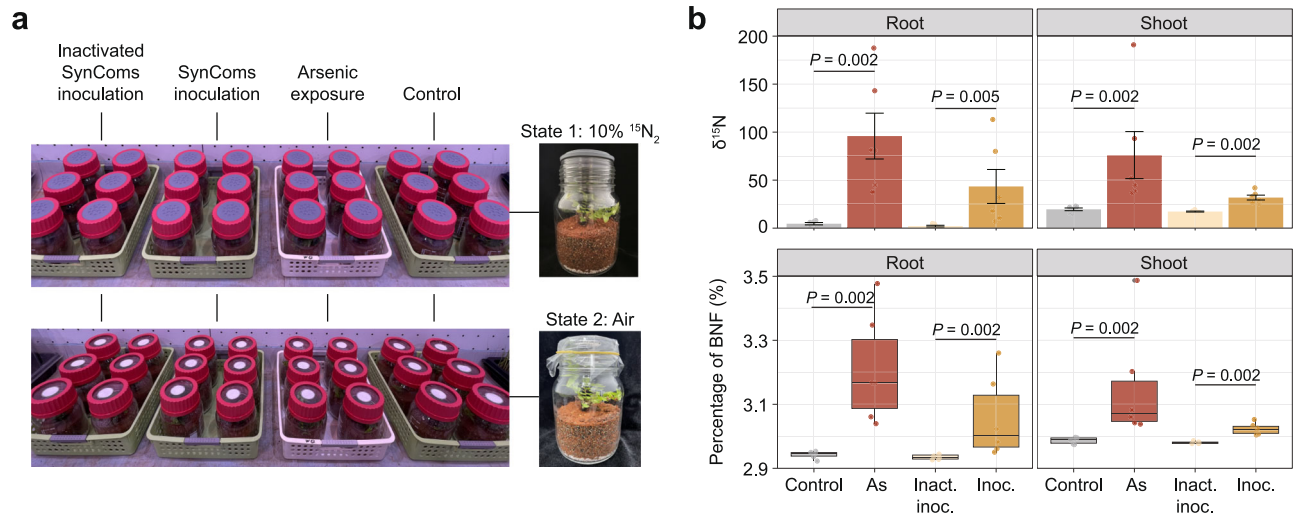

Fig. 5 | Contribution of biological nitrogen fixation under arsenic stress and synthetic communities (SynComs) to nitrogen nutrition of roots and shoot. **a** Overview of ^{15}N isotope tracer experiment. **b** $\delta^{15}N$ values and contribution of biological N fixation (BNF) to the total N accumulation in the roots and shoots of *Pteris vittata* ($n = 6$). Each data point represents a biologically independent replicate. *P* values were determined by the two-sided Wilcoxon test. In box plots, the center line represents the median, box edges delimit lower and upper quartiles and whiskers show the highest and lowest values.

regulated rhizosphere metabolites: (1) significant upregulation in the rhizosphere compared to bulk soil; (2) notable upregulation in the high-As rhizosphere in contrast to the low-As rhizosphere; (3) the absence of significant abundance changes between high- and low-As bulk soils; (4) significant upregulation in the high-As endosphere in contrast to the low-As endosphere; (5) presence within each rhizosphere or endosphere sample. The analysis revealed that β−1,2-mannotriose, L-asparagine, and catechin emerged as the prime candidates for As-regulated metabolites (Fig. 4a). L-valine, which met the first four criteria and exhibited moderate upregulation in the high-As endosphere ($P = 0.09$, Wilcoxon test, one-sided), was also regarded as a potentially As-regulated metabolite candidate.

To validate the accuracy of this method in identifying stress-regulated metabolites, a comprehensive targeted metabolomic analysis, focusing on 185 types of flavonoids (Supplementary Data 2), was conducted to assess changes in flavonoids within the rhizosphere soil with and without As exposure. The results of the 28-day pot experiment revealed that catechin was the only flavonoid significantly upregulated under As exposure, with its concentration reaching 0.1 nmol g^{-1}, a level significantly higher than that observed in the As-free control (undetectable) (Fig. 4b).

Furthermore, the ISCA microfluidic platform and flow cytometry (Supplementary Fig. 14) were used to directly quantify the chemotactic behavior of the diazotrophs *Bradyrhizobium* sp. J3 and *Rhizobium* sp. G5 on four As-regulated rhizospheric metabolites. Both *Bradyrhizobium* sp. J3 and *Rhizobium* sp. G5 exhibited positive chemotactic responses toward four metabolites (Wilcox-test, $p < 0.05$; Fig. 5c). Notably, the catechin and β−1,2-mannotriose exhibited the strongest chemoattractant effect on *Rhizobium* sp. G5, with chemotactic indexes of 5.38 ± 1.33 and 6.04 ± 1.63, respectively (Wilcox-test, one-side, paired, $p < 0.05$), and on *Bradyrhizobium* sp. J3, with chemotactic indexes of 4.39 ± 0.96 and 3.53 ± 0.76, respectively ($p < 0.05$) (Fig. 4c).

Contribution of arsenic to enhancing nitrogen fixation

The enhancement of biological N fixation by As exposure and diazotroph inoculation were further verified through the ^{15}N isotope tracer approach. The experiment included four treatments: (1) Inoculation of synthetic communities (SynComs) which consisted of two N-fixing bacteria (*Bradyrhizobium* sp. J3 and *Rhizobium* sp. G5); (2) Inoculation of de-activated SynComs; (3) Exposed to As (80 ppm); and (4) Control. The plant growth system was subject to five cycles of $^{15}N_2$ labeling; each cycle consisted of a closed state with 10% $^{15}N_2$ for 3 days and an open state exposed to air for 1 day, resulting in a cumulative $^{15}N_2$ labeling period of 15 days (Fig. 5a).

During the 15-day cultivation period, the contribution of biological N fixation to the total N accumulation in the roots and shoots of *Pteris vittata* was 2.94% and 2.99%, respectively. Despite the short cultivation period with $^{15}N_2$ labeling, As exposure significantly increased the proportion of biological N fixation. In the roots, the proportion of fixed N increased by an average of 0.27%, with a maximum increase of 0.54% to 3.48%. In the shoots, the proportion of fixed N increased by an average of 0.17%, with a maximum increase of 0.5% to 3.49%. Furthermore, plants inoculated with activated SynComs had a higher proportion of fixed N (average 3.06% in roots and 3.02% in shoots, with a maximum of 3.26% in roots and 3.05% in shoots) compared to plants inoculated with de-activated SynComs (average 2.93% in roots and 2.98% in shoots) (Fig. 5b).

Discussion

Pteris vittata thrives in As-contaminated soils, and its growth is mostly affected by a combination of nutrient limitation and As stress. Our field study (Fig. 1a) revealed that *Pteris vittata* actively enhanced N concentrations in its rhizosphere, suggesting a stress alleviation mechanism. The observed increase in total N concentration was attributed to an upregulation of biological N fixation, a crucial metabolic process carried out exclusively by prokaryotes[29]. Notably, elevated As stress significantly promoted N fixation in the rhizosphere, supported by upregulation of key N-fixation genes (e.g., *nifH*, *nifD*, and *nifK*), indicating a unique interaction between the host and diazotrophs (Fig. 1b). The greenhouse experiment further validated that N deficiency critically constrained plant growth in situ, which was ameliorated by As addition (Fig. 1d–f). These findings suggest an As-regulated mechanism of N acquisition in the rhizosphere of *Pteris vittata*. To decipher this mechanism, we employed an approach of comprehensive multi-omics (Supplementary Fig. 1). Diazotrophs in the rhizosphere were initially identified through metagenomic assembly ORFs using *nifH*-Palmscan, a tool designed for the recognition of *nifH* genes based on catalytic motifs. The isolation, cultivation and inoculation experiments then confirmed their capabilities in N fixation, As oxidation, and plant growth promotion, and identified *Rhizobium* sp. G5 and

https://doi.org/10.1038/s41467-024-54392-x

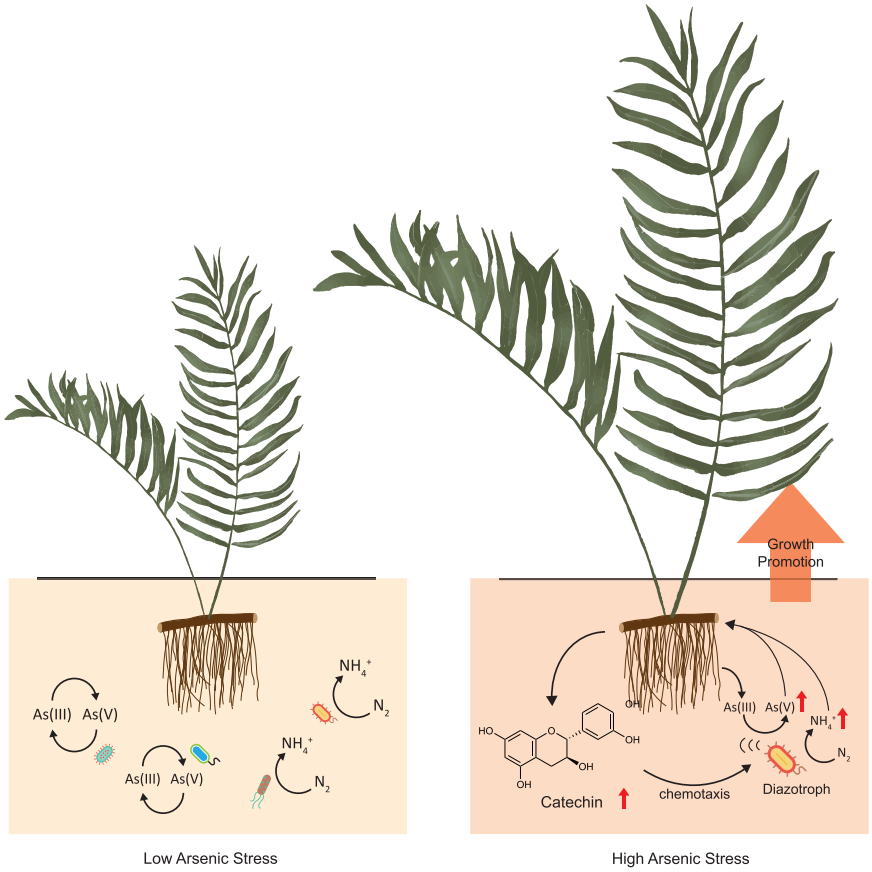

Fig. 6 | Proposed model for arsenic-regulated biological nitrogen fixation in *Pteris vittata*. In high-As soils, high content of chemoattractants in root exudates result in an enrichment of specific diazotrophic bacteria (e.g. *Bradyrhizobium* sp. J3 and *Rhizobium* sp. G5), which boosts plant growth and N uptake by enhancing biological N fixation.

Bradyrhizobium sp. J3 as key contributors. Further metabolomic analyses pinpointed key As-upregulated metabolites in the rhizosphere, including catechin, β–1,2-mannotriose, L-asparagine, and L-valine. Finally, the chemotactic interactions between these metabolites and key rhizosphere diazotrophs were confirmed on an ISCA microfluidic platform. Our findings support a mechanistic model that elevated As stress alters the composition of root exudates, particularly by enhancing the release of flavonoid signals such as catechin. This alteration of exudate composition facilitates the recruitment of key diazotrophs, including *Bradyrhizobium* sp. J3 and *Rhizobium* sp. G5, which enhances biological N fixation in the rhizosphere, thereby increasing N availability and promoting plant growth (Fig. 6).

Heavy metal can induce hormesis, a dose-response relationship in which low doses have a beneficial effect while high doses have an inhibitory effect[30], particularly in heavy-metal accumulators[31]. Previous studies have demonstrated that As can markedly promote the growth of *Pteris vittata*, even at As concentrations that are lethal to other plants species[3]. Our research reveals that the exposure to high As can induce enhanced biological N fixation in the rhizosphere of *Pteris vittata*, thereby facilitating N acquisition and promoting plant growth. This mechanism advances our understanding of hormesis and may holds substantial implications for stress alleviation in hyperaccumulators. *Pteris vittata* has evolved sophisticated mechanisms to cope with continuous As uptake from the environment. However, excessively high As concentrations can compromise chloroplast membrane integrity and lead to pinnae necrosis[32,33]. Hormesis likely serves as a stress alleviation strategy[34], wherein *Pteris vittata* regulates As concentrations in its fronds through modulation of aboveground biomass. Nitrogen is critical for the synthesis of proteins, plant growth, and chlorophyll synthesis[35]. The strategic investment in N acquisition is likely crucial for supporting the stress response mechanisms observed in *Pteris vittata*. Supporting this notion, long-term field studies showed an increased biomass and reduced As concentrations in the fronds of *Pteris vittata* under N treatment[36,37], underscoring the importance of N in enhancing plant resilience under high As exposure.

Flavonoids are pivotal regulators of plant growth and development, and play crucial roles in plant defense against biotic and abiotic stresses[38]. Previous studies have found that As exposure upregulated flavonoid biosynthesis pathway in *Pteris vittata*[27]. Our metabolomic analysis further identified catechin as a major flavonoid in the root exudates of *Pteris vittata*, with its release elevated by As stress. Chemotaxis assays demonstrated that catechin induces chemotactic responses in important rhizosphere diazotrophs, including *Bradyrhizobium* sp. J3 and *Rhizobium* sp. G5, suggesting it has a positive effect on diazotroph recruitment in the rhizosphere. This aligns with findings from extensive studies in *Fabaceae* plants, where the flavonoid functions as a root-released chemoattractant that promotes the multiplication of rhizobia on root surface[23].

In addition to direct chemotactic, catechin has been extensively characterized for their antimicrobial properties against both Gram-positive and Gram-negative bacteria[39]. The antimicrobial mechanisms include inducing bacterial cell membrane disruption and inhibiting cell wall synthesis[40]. Nevertheless, some microbial taxa can gain adaptive advantages by degrade flavonoid phytoalexins, allowing their persistence and colonization of plant hosts[41]. For instance, *Sclerotinia sclerotiorum* Circumvents flavonoid defenses by catabolizing flavonol glycosides and aglycones[42]. It is notable that both *Bradyrhizobium* and *Rhizobium* species have been documented to possess complete

catechin-degradation pathways[43,44], which potentially facilitate their successful colonization and niche expansion in the rhizosphere through the depletion of other resource competitors.

Moreover, β−1,2-mannotriose, L-asparagine, and L-valine were identified as additional effective chemo-attractants whose release is also modulated by As stress level. This observation suggests the potential existence of dual chemotaxis pathways, one towards nutrients and the other for sensing signal compounds[45]. While our findings provide evidence that catechin, β−1,2-mannotriose, L-asparagine and L-valine are crucial chemotactic agents, we cannot exclude the possibility that other root exudates may also play a role in regulating microbial community assembly under As stress. Further research is required to elucidate the underlying mechanisms and to understand how these compounds interact with others in shaping the community structure of diazotrophs.

Rhizobiales and Burkholderiales taxa are acknowledged as keystone groups in soil ecosystems, fostering universal mutualistic relationships with terrestrial plants[46] and playing a crucial role in host health[47]. They constitute core microbial populations in root-associated habitats of *Pteris vittata* and play a crucial role in promoting plant growth and As(III) oxidation[17,18]. Our metagenomic analysis revealed that 61% of diazotrophs in *Pteris vittata* rhizosphere are classified within the orders Rhizobiales and Burkholderiales. Interestingly, the *aioA* gene exhibited similar genetic traits and taxonomic overlap with the *nifH* gene within these groups. This homogeneous selection process may be co-mediated by root exudates and arsenite efflux. In addition to promoting the release of flavonoids, high As exposure can induce substantial arsenite efflux from the roots[48,49], creating arsenite-enriched zones within rhizosphere. This habitat could support the niche of diazotrophs that can harness arsenite and attracted by flavonoid chemoattractants, while inhibiting the growth of arsenite-intolerant organisms. The As oxidation and N fixation abilities observed in isolates from various genera within Rhizobiales and Burkholderiales further support this concept.

Besides, the supplementation of arsenite enhanced the N-fixing activity of *Rhizobium* sp. G5, suggesting a deeper coupling of As-metabolism and N fixation process. Since the biological N fixation relies on energy availability for reducing dinitrogen to ammonia, this biochemical process may be attributed to the ability of certain diazotrophs to capture energy from As oxidation. Previous studies reported that providing extra electrons via extracellular electron mediators enhanced biological N fixation of an anaerobic consortium[50]. Also, the addition of arsenite as an electron donor enhanced biological N fixation in As-rich soil and sediment[51]. Notably, *Rhizobium* G5 is capable of heterotrophic N fixation even in the absence of arsenite, but arsenite supplementation significantly enhances this process. Our finding suggests a distinct mechanism from the arsenite oxidation-dependent chemoautotrophic N fixation observed in *Serratia* species, as the activity of chemoautotrophic N fixation depends on the presence of arsenite[13]. Nevertheless, both processes indicate the potential of bacteria to utilize energy from As metabolism, highlighting the diversity of interactions between As and N metabolism in As-rich soils.

In summary, our research offers crucial insights into how As regulates N acquisition in *Pteris vittata*, offering a possible explanation for the hormesis phenomenon that As promotes the growth of this plant species. This discovery holds significant and promising implications for phytoremediation of As- or other heavy metals-contaminated soils. In the future, it is essential to clarify the exact mechanisms established, ranging from plant regulation to microbial responses in mutualistic symbiosis.

Methods

Sample collection and preprocessing

From June to September 2020, the root and rhizosphere soil samples of *Pteris vittata* ($n = 22$) and correspondingly adjacent bulk soils were collected to investigate the bacterial community. These samples were collected from three distinct sites in China: Zhuzhou, Hunan ($n = 7$, 27°45'35.2"N 113°12'59.2"E), Daye, Hubei ($n = 9$, 30°00'51.0"N, 114°48'24.0"E), and Wenshan, Yunnan ($n = 6$, 22°55'42.0"N, 104°31'28.0"E). The samples were taken randomly in specified areas within each site.

In September 2021, wild *Pteris vittata* plants with intact roots and rhizosphere soils and adjacent bulk soils (0.3 meters from the root) were also collected from the field sites with low-As (< 1000 ppm, $n = 10$) and high-As stress (> 1000 ppm, $n = 15$), respectively, in Wenshan, Yunnan (22°54'02.6"N, 104°23'08.4"E). The in-situ concentrations of heavy metals (metalloids) were evaluated using the Vanta™ Handheld XRF Series (Tokyo, Japan). In the laboratory, the rhizospheric soils and roots from *Pteris vittata* samples, alongside the collected bulk soils, were processed for subsequent metagenomic and metabolomic analyses.

Details of sampling procedure and sample processing are shown in Supplementary Information.

Determination of physicochemical properties of field samples

The physicochemical properties of bulk and rhizosphere soils were determined, including pH, total C and total N, dissolved organic C (DOC) and dissolved total N (DTN), NH_4-N and NO_3-N, total As, As(III) and As(V). The rhizosphere soil was characterized as the soil closely adhering to the roots. Additionally, the total As content in plant roots and fronds were also determined. Details for the determination of physicochemical properties are shown in Supplementary Information.

Amplicon sequence data processing

The 16S rRNA amplicon sequence underwent processing using the QIIME2[52] (v2021.9) pipeline, following a meticulous protocol: Primers were excised from the sequences with the cutadapt plugin after the quality of the sequences was assessed. Representative amplicon sequence variants (ASVs) were generated and enumerated using the DADA2 (v1.20.0) denoise-paired plugin. In addition, a classifier was trained utilizing the small subunit ribosomal RNA (SSU rRNA) gene dataset from the GTDB[53] database r207_v2 release (https://gtdb.ecogenomic.org/releases/release207) and employed to assign taxonomic classifications to the ASVs with a 0.8 confidence threshold. The differential analysis of ASV abundance between different treatments using the R package 'Deseq2'[54].

Metagenomic annotation and abundance profiling

Metagenomic raw reads were subjected to quality control, primer clipping, and paired-end sequence alignment using Fastp[55] with the parameters (-q 20). Subsequently, metaSPAdes[56] was employed to assemble quality-controlled reads from individual samples, with parameters (–meta). All contigs were merged and contigs with length less than 300 bp were removed.

To comprehensively assess microbial dark matter, ORFs were predicted from contigs using Prodigal[57] v2.6.3. Sequences shorter than 100 residues were removed, resulting in a redundant reference set of 325,757,514 coding DNA sequences (CDS). The redundancy was reduced by clustering at 95% sequence identity and 95% minimum coverage of the shorter sequence using mmseq2[58] (parameters: –cov-mode 1 –cluster-mode 2), resulting in the non-redundant reference set comprising 168,738,358 representative CDS. All metagenomes were subsequently mapped to the representative CDS using bwa-mem2[59] v2.2.1, and the results were filtered to retain only alignments with a percentage identity of ≥ 97% aligned. The depth of CDS was evaluated by calculating the mean and variances of mapped reads. Additionally, the abundance profile was determined by normalization with the library of mapped reads.

The *nifH*, *nifD* and *nifK* and other genes related to the N cycle were aligned against the NcycDB database[60] using the diamond[61] v2.0.15

with following parameters: -k 1 -e 0.00001 –id 50 –query-cover 80 –more-sensitive. To annotate functional genes related to As metabolism, an alignment was conducted against an As-related gene database[62], including nine key As-resistance and metabolism genes: *aioA*, *acr3*, *arsB*, *arsC* (*grx*), *arsC* (*trx*), *arsD*, *arsM*, *arrA*, and *arxA*, using the same method and parameters.

Development of *nifH*-Palmscan

Sequence logos can be represented formally as position-specific scoring matrices (PSSMs), allowing for efficient computational searches for ungapped matches[63]. Palmscan implemented this approach to automate the identification of palmprints[28]. Palmscan aligns known motif PSSMs to nucleotide or amino acid sequences, reporting hits where motifs have high log-odds scores and are separated by distances similar to those in known palm domains.

To ensure precise identification of *nifH* sequences within metagenomes, its palm domain was descripted in 3 highly conservative motifs: a site for ATP-binding and two for Fe-S factor binding. In parallel, the heuristic parameters of Palmscan were fine-tuned based on our prior understanding of the *nifH* gene, which encompassed aspects including the length, order, and span of motifs. The source code is available on Github (https://github.com/JaphethLin/nifH_palmscan).

For PSSMs modeling, multiple sequence alignments (MSAs) for each motif were constructed as follows. First, a seed alignment was manually constructed on a base dataset. Second, the resulting PSSM was employed to search datasets containing *nifH* sequences. Third, integrating new *nifH* sequences into the base dataset and deduplicating. The process was iterated until no further improvement was achieved. Details for training and validation datasets are presented in Supplementary Information.

In the evaluation of the palmprint identification and classification algorithms, two pivotal accuracy metrics are employed: Positive Predictive Value (PPV) and False Discovery Rate (FDR). The PPV signifies the ratio of accurate predictions to the overall number of predictions, whereas FDR reflects the proportion of erroneous predictions among all predictions made.

Phylogenetic analysis of *nifH* gene

For each individual tree, the following steps were performed. Amino acid sequences were first aligned using MAFFT[64] v7.471, with the (-auto option). The alignments were subsequently trimmed using TrimAl[65] v1.2.59, with the (-gappyout option). Maximum-likelihood trees were constructed using IQ-TREE[66] v2.0.5105, employing the best-fit models and generating 1000 ultrafast bootstraps. The produced trees were then visualized and improved using Interactive Tree of Life[67] (iTOL).

Metabolomic analyses

To recognize key rhizosphere metabolites in response to stress, both targeted and untargeted metabolomics approaches were applied to detect metabolites in soil and plant roots. For untargeted metabolomics analysis, 50 soil samples (5 g each of bulk and rhizosphere soil) and 25 root samples (200 mg) were collected from 25 wild *Pteris vittata* plants and proportionally extracted using pre-cooled acetonitrile: methanol: H_2O (2:2:1, v/v/v). This mixed solvent system was selected with the aim of enhancing the extraction efficiency of compounds with varying polarities, effectively penetrating cell membranes, preserving metabolite stability, and ensuring compatibility with mass spectrometry for high-quality spectral data acquisition. After centrifugation at 10,000 × *g* for 10 min, the supernatant was harvested for LC-MS/MS measurement. Quality control (QC) samples were prepared by pooling equal aliquots from all samples collected. One QC sample was injected prior to the analysis and after every ten runs to assess the analytical variance. Untargeted metabolomics was performed with Vanquish UHPLC system fitted with a Q Exactive HF-X mass spectrometer (Thermo Fisher Scientific, USA). For targeted metabolomics analysis, 100 mg of rhizosphere soil were collected from *Pteris vittata* grown in control ($n = 6$) and As-amended soil ($n = 6$) and extracted with 70% MeOH. The targeted metabolomics analysis was conducted with QTRAP 6500+ system (SCIEX, USA). Both chromatographic analyses were conducted using a Waters ACQUITY UPLC HSS T3 column (1.8 µm, 100 mm × 2.1 mm). While this approach satisfies the requirements of our research, it is important to recognize that relying solely on a C18 column for broad-spectrum untargeted metabolite separation and identification has its limitations, potentially impacting the detection of molecules with extreme hydrophobicity and high polarity. Detailed parameters of the collection and detection for metabolites in targeted and untargeted metabolomics are provided in Supplementary Information.

Metabolomic data process

In untargeted metabolomics analysis, the raw MS data were converted to mzXML format by MSConvert in ProteoWizard software package[68] (v3.0) and processed by XCMS[69] (v3.2) for peak picking and alignment. The XCMS settings were as follows: method = “centWave”, ppm = 15, peakwidth = c(5,30), mzwid = 0.015, mzdiff = 0.01, and bw = 2.

The peak areas of all detected ions were normalized according to robust locally-estimated scatterplot smoothing (LOESS) signal correction[70] based on QC samples (Details for QC sample are available in SI). After normalization, the ion peaks with relative standard deviations > 30% in the in all QC samples were deleted.

Metabolite secondary identification was performed by accurate mass and MS/MS matching against the spectra data from an in-house metabolite library of standard compounds (Shanghai Personal Biotechnology, Shanghai, China) and public databases (HMDB[71], MassBank[72], LipidMaps[73], mzCloud[74] and KEGG[75]). The MS/MS spectral similarity was represented using the cosine score. The metabolite with the highest score is considered as the identified compound. Among these, 968 metabolites passed secondary identification were used for downstream statistical analysis.

Key metabolite identification

The R package Ropls[76] (v1.22.0) was used for scaling and multivariate statistical analyses of all normalized MS data. In detail, adaptive scaling transformation was employed to scale the data, followed by Orthogonal Partial Least Squares Discriminant Analysis (OPLS-DA) to recognize differential metabolites between between the pairwise sample groups. Consequently, we conducted four pairwise comparisons among the sample groups, corresponding to criteria 1-4 mentioned above:

1. high-arsenic rhizosphere soil vs. high-arsenic bulk soil.
2. high-arsenic rhizosphere soil vs. low-arsenic rhizosphere soil.
3. high-arsenic bulk soil vs. low-arsenic bulk soil.
4. high-arsenic root vs. low-arsenic root.

Differential metabolites from each pairwise sample group comparison were recognized based on the following screening thresholds: (1) a Variable Important for the Projection (VIP) score > 1 for the first PC of the OPLS-DA model, and (2) P-value < 0.05. Key metabolites were then identified by applying set intersection (set operations) to the statistically significant metabolites recognized by each criterion.

Growth promotion ability of arsenic

The seedlings of *Pteris vittata* with 6–7 fronds and 3–4 cm size stage were used for the pot experiments. Seedling development is detailed in the Supplementary Information. The experimental soil was collected from the field sampling site in Wenshan field without heavy metal pollution. The experimental soil was mixed with 20% N-free Hoagland's nutrient solution and either Na_2HAsO_4 solution (Sigma-Aldrich, St. Louis, Mo, USA) or $(NH_4)_2SO_4$ solution, and then pre-incubated for 2 months at 60% field capacity to obtain the treated soils (80 ppm As-amended soil and 50 ppm N-amended soil). Each seedling of *Pteris*

vittata was grown in a pot (16 cm in average diameter and 15 cm in height) containing 2.5 liters of pre-treated soil for 50 days. Soil moisture was maintained at 60% field capacity with deionized water in a growth chamber with a 12-h light/12-h dark cycle at 28 °C.

Growth promotion potential of isolated diazotrophs

Inoculation of N_2-fixing bacterial strains into the YM broth was conducted at 28 °C on a shaker at 120 rpm for 48 h. Following cultivation, the bacterial suspension was centrifuged at 6000 × *g* for 5 min. The cell pellet was washed three times using sterile phosphate-buffered saline (PBS) and resuspended in PBS buffer to create a cell suspension (10^8 cells mL^{-1}). The experiment consisted of five treatments:

(i) Inoculation: *Rhizobium* sp. G5 (designated as Rhi. Inoc.)
(ii) Inoculation: *Mesorhizobium* sp. M12 (designated as Mes. Inoc.)
(iii) Inoculation: *Bradyrhizobium* sp. J3 (designated as Brad. Inoc.)
(iv) Inoculation: *Cupriavidus* sp. N2 (designated as Cup. Inoc.)
(v) Control group: No bacterial inoculation (designated as control).

One seedling of *Pteris vittata* was grown in each pot (16 cm in average diameter and 15 cm in height) containing 2.5 liters of pre-sterilized soil that had been pre-treated with 20% N-free Hoagland's nutrient solution. Soil moisture was maintained at 60% field capacity with deionized water in a growth chamber with a 12-h light/12-h dark cycle at 28 °C. A bacterial suspension (or de-activated bacterial suspension for control) (3 mL) was applied to each potted plant at transplanting, and this was repeated on the 7th day. The plants were not fertilized but watered every 2 d with 50 mL deionized water per pot. After 40-d growth, rhizosphere soil, root, and stem samples were collected from each treatment, and measurements were taken for total plant biomass, total N content, plant height, *nifH* content, and 16 s RNA.

Quantitative PCR of *nifH* gene

Quantitative PCR (qPCR) was then performed on a LightCycler 480 II (Roche, Basel, Switzerland) to determine the copy numbers of the *nifH* gene. The specific primers and cycling parameters used for qPCR are listed in Supplementary Table 6. The amplification efficiency ranged from 91% to 95%, with the correlation coefficients (R^2) of the standard curves exceeding 0.99.

Assessment of arsenic oxidation and nitrogen fixation capacity

In order to study As(III) oxidation activity, selected strains were cultured in N-rich and N-free media for 3 and 9 d, and were destructively collected daily and every 3 d, respectively, and the values of optical density (OD) were recorded. Arsenic speciation was determined after filtration through a 0.22-μm sterile filter membrane. Details for determination of As species are given in the Supplementary Information.

To verify the N_2-fixing capability of the strains, their growth in liquid N-free medium (Mannose, 10 g L^{-1}; KH_2PO_4, 200 mg L^{-1}; $MgSO_4$, 200 mg L^{-1}; $CaCl_2$, 100 mg L^{-1}; NaCl, 100 mg L^{-1}) was confirmed after two subcultures. Strains with an OD value exceeding 0.5 were subsequently tested for nitrogenase activity. The nitrogenase activity of the strains was assessed using the enzyme-linked immunosorbent assay kit extraction method (Qingdao Kechuang Quality Testing Co., Ltd, Qingdao, Shandong, China). This involved employing the double antibody sandwich technique, whereby a micropore is coated with purified monoclonal nitrogenase antibody to prepare a solid-phase antibody. Nitrogenase was then sequentially introduced to the coated micropore and combined with nitrogenase antibody labeled with horseradish peroxidase (HRP) to form an antibody–antigen–enzyme-labeled complex. Following thorough washing, tetramethylbenzidine (TMB) was added for color development. It exhibits a blue color catalyzed by HRP, which turns yellow in the presence of acid; the intensity of the color is directly proportional to nitrogenase activity. Absorbance was measured at 450 nm using a MD SpectraMax 190 microplate reader (Molecular Devices, CA, USA), and nitrogenase activity was determined based on a standard curve.

Laboratory chemotaxis experiments with diazotroph isolates

Overnight cultures of diazotrophs *Bradyrhizobium* sp. J3 and *Rhizobium* sp. G5 (OD_{600} = 0.5) were diluted 1:1000 in 1% YM broth (in autoclaved PBS at pH 7.2), and further incubated for 3 h. Subsequently, the cultures were diluted 10-fold in PBS to achieve a cell suspension with a concentration of 3–4 × 10^4 cells mL^{-1}.

To explore the chemotactic capability of diazotrophic isolates in laboratory settings and natural diazotroph assemblages in the rhizosphere, a chemotaxis assay using the microfluidic platform ISCA[77] was employed. This device consists of an array of wells connected to the external environment through a port (Supplementary Fig. 14). Potential chemoattractants were loaded into the wells, and upon deployment of the ISCA, they diffused out to create concentration gradients similar to natural chemical hotspots. Motile and chemotactic cells could then navigate these gradients and migrate into the wells for sampling. Each experiment utilized four ISCAs deployed simultaneously (n = 4), with each ISCA accommodating five technical replicates of five different treatments conducted concurrently. Chemotaxis experiments were conducted using key rhizospheric metabolites identified (Carbohydrate: mannotriose; Amino acid: L-asparagine, L-valine; Flavonoid: catechin; all at 1 mM).

In laboratory-based chemotaxis experiments, ISCAs were placed in sterile plastic trays and incubated at 25 °C for 2 h after adding 240 mL of cell suspension[78]. Post-incubation, the contents of ISCA wells were retrieved using a 1-mL syringe fitted with a 27 G needle (Terumo, Sydney, Australia). Approximately 550 μL, obtained by pooling the contents of five wells per ISCA, was then subjected to immediate flow cytometry analysis.

Samples for flow cytometry were stained with SYTO 9 Green fluorescent (Thermo Fisher) and Propidium iodide (PI) red fluorescent (Thermo Fisher), and CountBright™ absolute counting beads (1000 beads μL^{-1}; Thermo Fisher) were added for counting. The samples were then incubated for 15 min in the dark and analyzed on a DB FACS-Melody Cell Sorter (DB, Franklin Lakes, USA). Each sample was assessed for forward scatter (FSC), side scatter (SSC), red fluorescence (PI), and green fluorescence (SYTO 9), with analysis conducted at a flow rate of 50 μL min^{-1}. Living microbial cells were profiled based on SSC, PI Red (utilized to detect dead cells) and SYTO 9 Green (utilized to detect live cells) fluorescence. To quantify the intensity of chemotaxis, the Ic was determined by dividing the number of cells in a specific treatment by the number in the PBS control[77]. Ic values > 1 indicate attraction, whereas Ic values < 1 suggest repulsion.

^{15}N isotope tracing experiment

To verify the enhancement of biological N fixation by As and diazotrophs, a $^{15}N_2$ enrichment incubation assay was conducted. The mixture of 350 mL of soil and vermiculite (v:v = 5:2) was added to each 750-mL glass anaerobic bottle. The experimental soil was pre-treated by 20% N-free Hoagland's nutrient solution with or without Na_2HAsO_4 solution. The experiment included four treatments: (1) Inoculation of SynComs which consisted of two N-fixing bacteria (*Bradyrhizobium* sp. J3 and *Rhizobium* sp. G5); (2) Inoculation of de-activated SynComs; (3) Exposed to As (80 ppm); and (4) Control (Fig. 5a). After transplanting *Pteris vittata* seedlings, 3 mL bacterial suspension of isolated diazotrophs (or de-activated bacterial suspension in the control treatment) added to each of the bottles of treatments (1) and (2). Following a 10-day pre-culturing period, the bottles were sealed, and 10% (v/v) of the headspace was replaced with $^{15}N_2$, which was kept for 3 d. The bottles were then aerated for 1 d. After 5 cycles, the roots and shoots of the plants were destructively sampled, freeze-dried, and analyzed for ^{15}N isotope content. The $\delta^{15}N$ value of plant tissues (finely ground) was

determined by an Isoprime 100 isotope mass spectrometer (Isoprime, Cheadle, United Kingdom).

Statistics and reproducibility

No data were excluded from the analyses. The investigators were blinded to allocation during experiments and outcome assessment.

Reporting summary

Further information on research design is available in the Nature Portfolio Reporting Summary linked to this article.

Data availability

The raw sequence data generated in this study have been deposited in the NCBI database under accession code PRJNA1067393. The MS data generated in this study have been deposited in the Metabolomics Workbench database under accession code PR002175 (https://doi.org/10.21228/M8GJ7D). The model-training and annotation data used in this study are available in the NCBI database (https://ftp.ncbi.nih.gov/blast/db), the GTDB database (https://data.ace.uq.edu.au/public/gtdb/data/releases/release207) and the custom protein databases of representative NifH sequences under accession code https://doi.org/10.26180/c.5230745 (ref. 79). Source data are provided with this paper.

Code availability

NifH-Palmscan (v1.0.0) are available at https://github.com/JaphethLin/nifH_palmscan (https://doi.org/10.5281/zenodo.13956241). The scripts used to generate the figures are described at https://github.com/JaphethLin/PVBNF (https://doi.org/10.5281/zenodo.13957208).

References

1. Qi, X. et al. A well-resolved fern nuclear phylogeny reveals the evolution history of numerous transcription factor families. *Mol. Phylogenet. Evol.* **127**, 961–977 (2018).
2. Ma, L. Q. et al. A fern that hyperaccumulates arsenic. *Nature* **409**, 579–579 (2001).
3. Zhao, F. et al. Arsenic in the hyperaccumulator *Pteris vittata*: A review of benefits, toxicity, and metabolism. *Sci. Total Environ.* **896**, 165232 (2023).
4. Li, Y. et al. Synergistic impacts of arsenic and antimony co-contamination on diazotrophic communities. *Microb. Ecol.* **84**, 44–58 (2022).
5. Sun, X. et al. Microbially mediated sulfur oxidation coupled with arsenate reduction within oligotrophic mining-impacted habitats. *ISME J.* **18**, 1 (2024).
6. Norman, J. S. & Friesen, M. L. Complex N acquisition by soil diazotrophs: how the ability to release exoenzymes affects N fixation by terrestrial free-living diazotrophs. *ISME J.* **11**, 315–326 (2017).
7. Li, Y. et al. Characterization of diazotrophic root endophytes in Chinese silvergrass (*Miscanthus sinensis*). *Microbiome* **10**, 186 (2022).
8. Li, Y. et al. Variations on the diazotrophic community in the rhizosphere soil of three dominant plant species in a lead–zinc mine area. *Plant Soil* **489**, 155–175 (2023).
9. Wang, W. et al. Intercropping efficiency of *Pteris vittata* with two legume plants: Impacts of soil arsenic concentrations. *Ecotox. Environ. Safe.* **259**, 115004 (2023).
10. Tang, L. et al. Fava bean intercropping with *Sedum alfredii* inoculated with endophytes enhances phytoremediation of cadmium and lead co-contaminated field. *Environ. Pollut.* **265**, 114861 (2020).
11. Saad, R. F., Echevarria, G., Rodríguez-Garrido, B., Kidd, P. & Benizri, E. A two-year field study of nickel-agromining using *Odontarrhena chalcidica* co-cropped with a legume on an ultramafic soil: temporal variation in plant biomass, nickel yields and taxonomic and bacterial functional diversity. *Plant Soil* **461**, 471–488 (2021).
12. Garcia-Dominguez, E., Mumford, A., Rhine, E. D., Paschal, A. & Young, L. Y. Novel autotrophic arsenite-oxidizing bacteria isolated from soil and sediments: Novel autotrophic arsenite-oxidizing bacteria. *FEMS Microbiol. Ecol.* **66**, 401–410 (2008).
13. Li, Y. et al. *Serratia* spp. are responsible for nitrogen fixation fueled by As(III) oxidation, a novel biogeochemical process identified in mine tailings. *Environ. Sci. Technol.* **56**, 2033–2043 (2022).
14. Bais, H., Weir, T., Perry, L., Gilroy, S. & Vivanco, J. The role of root exudates in rhizosphere interactions with plants and other organisms. *Annu. Rev. Plant Biol.* **57**, 233–266 (2006).
15. Ling, N., Wang, T. & Kuzyakov, Y. Rhizosphere bacteriome structure and functions. *Nat. Commun.* **13**, 836 (2022).
16. Shi, S. et al. OsHAC1;1 and OsHAC1;2 function as arsenate reductases and regulate arsenic accumulation. *Plant Physiol.* **172**, 1708–1719 (2016).
17. Sun, X. et al. Arsenic (As) oxidation by core endosphere microbiome mediates As speciation in *Pteris vittata* roots. *J. Hazard. Mater.* **454**, 131458 (2023).
18. Huang, D. et al. Bacteria associated with *Comamonadaceae* are key arsenite oxidizer associated with *Pteris vittata* root. *Environ. Pollut.* **349**, 123909 (2024).
19. Liu, H., Brettell, L. E., Qiu, Z. & Singh, B. K. Microbiome-mediated stress resistance in plants. *Trends Plant Sci.* **25**, 733–743 (2020).
20. Gough, C. et al. Specific flavonoids promote intercellular root colonization of *Arabidopsis thaliana* by *Azorhizobium caulinodans* ORS571. *Mol. Plant-Microbe Interact.* **10**, 560–570 (1997).
21. Webster, G. et al. The flavonoid naringenin stimulates the intercellular colonization of wheat roots by *Azorhizobium caulinodans*. *Plant Cell Environ.* **21**, 373–383 (1998).
22. Huang, A. C. et al. A specialized metabolic network selectively modulates Arabidopsis root microbiota. *Science* **364**, 6440 (2019).
23. Wang, L. et al. Multifaceted roles of flavonoids mediating plant-microbe interactions. *Microbiome* **10**, 233 (2022).
24. Yu, P. et al. Plant flavones enrich rhizosphere Oxalobacteraceae to improve maize performance under nitrogen deprivation. *Nat. Plants* **7**, 481–499 (2021).
25. He, D. et al. Flavonoid-attracted *Aeromonas* sp. from the *Arabidopsis* root microbiome enhances plant dehydration resistance. *ISME J.* **16**, 2622–2632 (2022).
26. Hou, D. et al. Metal contamination and bioremediation of agricultural soils for food safety and sustainability. *Nat. Rev. Earth Environ.* **1**, 366–381 (2020).
27. Han, Y. H. et al. Arsenic-enhanced plant growth in As-hyperaccumulator *Pteris vittata*: metabolomic investigations and molecular mechanisms. *Sci. Total Environ.* **926**, 171922 (2024).
28. Edgar, R. C. et al. Petabase-scale sequence alignment catalyses viral discovery. *Nature* **602**, 142–147 (2022).
29. Coale, T. H. et al. Nitrogen-fixing organelle in a marine alga. *Science* **384**, 217–222 (2024).
30. Agathokleous, E., Kitao, M. & Calabrese, E. J. Hormesis: a compelling platform for sophisticated plant science. *Trends Plant Sci.* **24**, 318–327 (2019).
31. Calabrese, E. J. & Agathokleous, E. Accumulator plants and hormesis. *Environ. Pollut.* **274**, 116526 (2021).
32. Li, W.-X., Chen, T.-B., Huang, Z.-C., Lei, M. & Liao, X.-Y. Effect of arsenic on chloroplast ultrastructure and calcium distribution in arsenic hyperaccumulator *Pteris vittata* L. *Chemosphere* **62**, 803–809 (2006).
33. Han, Y.-H. et al. Arsenic accumulation and distribution in *Pteris vittata* fronds of different maturity: Impacts of soil As concentrations. *Sci. Total Environ.* **715**, 135298 (2020).
34. Zhang, J. et al. Hormesis in the heavy metal accumulator plant *Tillandsia ionantha* under Cd exposure: Frequency and function of different biomarkers. *Sci. Total Environ.* **889**, 164328 (2023).

35. Maathuis, F. J. Physiological functions of mineral macronutrients. *Curr. Opin. Plant Biol.* **12**, 250–258 (2009).
36. Matzen, S. L., Olson, A. L. & Pallud, C. E. Soil texture and climate limit cultivation of the arsenic hyperaccumulator *Pteris vittata* for phytoextraction in a long-term field study. *J. Hazard. Mater.* **436**, 129151 (2022).
37. Wu, J., Zhang, H., Cheng, X. & Liu, G. Nitrogen addition stimulates litter decomposition rate: from the perspective of the combined effect of soil environment and litter quality. *Soil Biol. Biochem.* **179**, 108992 (2023).
38. Nakabayashi, R. et al. Enhancement of oxidative and drought tolerance in *Arabidopsis* by overaccumulation of antioxidant flavonoids. *Plant J.* **77**, 367–379 (2014).
39. Hartmann, M. et al. Damage of the bacterial cell envelope by antimicrobial peptides gramicidin S and PGLa as revealed by transmission and scanning electron microscopy. *Antimicrob. Agents Chemother.* **54**, 3132–3142 (2010).
40. Górniak, I., Bartoszewski, R. & Króliczewski, J. Comprehensive review of antimicrobial activities of plant flavonoids. *Phytochem. Rev.* **18**, 241–272 (2019).
41. Zhou, H. et al. Pseudomonas syringae type III effector HopZ1 targets a host enzyme to suppress isoflavone biosynthesis and promote infection in soybean. *Cell Host Microbe* **9**, 177–186 (2011).
42. Chen, J., Ullah, C., Reichelt, M., Gershenzon, J. & Hammerbacher, A. Sclerotinia sclerotiorum Circumvents flavonoid defenses by catabolizing flavonol glycosides and aglycones. *Plant Physiol.* **180**, 1975–1987 (2019).
43. Gajendiran, N. & Mahadevan, A. Utilization of catechin by *Rhizobium* sp. *Plant Soil* **108**, 263–266 (1988).
44. Hopper, W. & Mahadevan, A. Degradation of catechin by *Bradyrhizobium japonicum*. *Biodegradation* **8**, 159–165 (1997).
45. Pandya, S., Iyer, P., Gaitonde, V., Parekh, T. & Desai, A. Chemotaxis of *Rhizobium* sp. S2 towards *Cajanus cajan* root exudate and its major components. *Curr. Microbiol.* **38**, 205–209 (1999).
46. Banerjee, S., Schlaeppi, K. & Van Der Heijden, M. G. A. Keystone taxa as drivers of microbiome structure and functioning. *Nat. Rev. Microbiol.* **16**, 567–576 (2018).
47. Hayat, R., Ali, S., Amara, U., Khalid, R. & Ahmed, I. Soil beneficial bacteria and their role in plant growth promotion: a review. *Ann. Microbiol.* **60**, 579–598 (2010).
48. Chen, Y., Fu, J., Han, Y., Rathinasabapathi, B. & Ma, L. Q. High As exposure induced substantial arsenite efflux in As-hyperaccumulator *Pteris vittata*. *Chemosphere* **144**, 2189–2194 (2016).
49. Han, Y.-H., Fu, J.-W., Chen, Y., Rathinasabapathi, B. & Ma, L. Q. Arsenic uptake, arsenite efflux and plant growth in hyperaccumulator *Pteris vittata*: Role of arsenic-resistant bacteria. *Chemosphere* **144**, 1937–1942 (2016).
50. Dey, S. et al. Promotion of biological nitrogen fixation activity of an anaerobic consortium using humin as an extracellular electron mediator. *Sci. Rep.* **11**, 6567 (2021).
51. Li, Y. et al. *Thiobacillus* spp. and *Anaeromyxobacter* spp. mediate arsenite oxidation-dependent biological nitrogen fixation in two contrasting types of arsenic-contaminated soils. *J. Hazard. Mater.* **443**, 130220 (2023).
52. Bolyen, E. et al. Reproducible, interactive, scalable and extensible microbiome data science using QIIME 2. *Nat. Biotechnol.* **37**, 852–857 (2019).
53. Parks, D. H. et al. A complete domain-to-species taxonomy for bacteria and archaea. *Nat. Biotechnol.* **38**, 1079–1086 (2020).
54. Love, M. I., Huber, W. & Anders, S. Moderated estimation of fold change and dispersion for RNA-seq data with DESeq2. *Genome Biol.* **15**, 550 (2014).
55. Chen, S., Zhou, Y., Chen, Y. & Gu, J. Fastp: an ultra-fast all-in-one FASTQ preprocessor. *Bioinformatics* **34**, i884–i890 (2018).
56. Nurk, S., Meleshko, D., Korobeynikov, A. & Pevzner, P. A. metaSPAdes: a new versatile metagenomic assembler. *Genome Res.* **27**, 824–834 (2017).
57. Hyatt, D. et al. Prodigal: prokaryotic gene recognition and translation initiation site identification. *BMC Bioinform.* **11**, 119 (2010).
58. Steinegger, M. & Söding, J. MMseqs2 enables sensitive protein sequence searching for the analysis of massive data sets. *Nat. Biotechnol.* **35**, 1026–1028 (2017).
59. Vasimuddin, Md., Misra, S., Li, H. & Aluru, S. Efficient architecture-aware acceleration of BWA-MEM for multicore systems. IEEE International Parallel and Distributed Processing Symposium (IPDPS) pp, 314–324 (2019).
60. Tu, Q., Lin, L., Cheng, L., Deng, Y. & He, Z. NCycDB: a curated integrative database for fast and accurate metagenomic profiling of nitrogen cycling genes. *Bioinformatics* **35**, 1040–1048 (2019).
61. Buchfink, B., Reuter, K. & Drost, H. Sensitive protein alignments at tree-of-life scale using DIAMOND. *Nat. Methods* **18**, 366–368 (2021).
62. Dunivin, T. K., Yeh, S. Y. & Shade, A. A global survey of arsenic-related genes in soil microbiomes. *BMC Biol.* **17**, 45 (2019).
63. Stormo, G. D., Schneider, T. D. & Gold, L. Use of the 'Perceptron' algorithm to distinguish transational initiation sites in E. *coli*. *Nucleic Acids Res.* **10**, 2997–3011 (1982).
64. Katoh, K. & Standley, D. M. A simple method to control over-alignment in the MAFFT multiple sequence alignment program. *Bioinformatics* **32**, 1933–1942 (2016).
65. Capella-Gutiérrez, S., Silla-Martínez, J. M. & Gabaldón, T. TrimAl: a tool for automated alignment trimming in large-scale phylogenetic analyses. *Bioinformatics* **25**, 1972–1973 (2009).
66. Nguyen, L., Schmidt, H. A., Von Haeseler, A. & Minh, B. Q. IQ-TREE: A fast and effective stochastic algorithm for estimating maximum-likelihood phylogenies. *Mol. Biol. Evol.* **32**, 268–274 (2015).
67. Letunic, I. & Bork, P. Interactive Tree Of Life (iTOL) v5: an online tool for phylogenetic tree display and annotation. *Nucleic Acids Res.* **49**, W293–W296 (2021).
68. Chambers, M. C. et al. A cross-platform toolkit for mass spectrometry and proteomics. *Nat. Biotechnol.* **30**, 918–920 (2012).
69. Smith, C. A., Want, E. J., O'Maille, G., Abagyan, R. & Siuzdak, G. XCMS: processing mass spectrometry data for metabolite profiling using nonlinear peak alignment, matching, and identification. *Anal. Chem.* **78**, 779–787 (2006).
70. Gagnebin, Y. et al. Metabolomic analysis of urine samples by UHPLC-QTOF-MS: Impact of normalization strategies. *Anal. Chim. Acta* **955**, 27–35 (2017).
71. Wishart, D. S. et al. HMDB 5.0: the human metabolome database for 2022. *Nucleic Acids Res.* **50**, D622–D631 (2022).
72. Horai, H. et al. MassBank: a public repository for sharing mass spectral data for life sciences. *J. Mass Spectrom.* **45**, 703–714 (2010).
73. Sud, M. et al. LMSD: LIPID MAPS structure database. *Nucleic Acids Res.* **35**, D527–D532 (2007).
74. Wang, J., Peake, D. A., Mistrik, R., Sanders, M. & Huang, Y. Mass spectral databases for LC/MS- and GC/MS-based metabolomics: State of the field and future prospects. *Trac-Trends Anal. Chem.* **78**, 23–35 (2016).
75. Kanehisa, M., Furumichi, M., Tanabe, M., Sato, Y. & Morishima, K. KEGG: new perspectives on genomes, pathways, diseases and drugs. *Nucleic Acids Res.* **45**, D353–D361 (2017).
76. Thévenot, E. A., Roux, A., Xu, Y., Ezan, E. & Junot, C. Analysis of the human adult urinary metabolome variations with age, body mass index, and gender by implementing a comprehensive workflow for univariate and OPLS statistical analyses. *J. Proteome Res.* **14**, 3322–3335 (2015).
77. Lambert, B. S. et al. A microfluidics-based in situ chemotaxis assay to study the behaviour of aquatic microbial communities. *Nat. Microbiol.* **2**, 1344–1349 (2017).

78. Hallstrøm, S. et al. Chemotaxis may assist marine heterotrophic bacterial diazotrophs to find microzones suitable for N_2 fixation in the pelagic ocean. *ISME J.* **16**, 2525–2534 (2022).
79. Chen, Y. J. et al. Metabolic flexibility allows bacterial habitat generalists to become dominant in a frequently disturbed ecosystem. *ISME J.* **15**, 2986–3004 (2021).

Acknowledgements

This work was supported by the National Science Foundation of China (grants 41991334 to J.X.), Science and Technology Program of Zhejiang Province (2022C02046 to J.X.), the 111 Project (B17039 to J.X.), and China Agriculture Research System (CARS-01 to J.X.).

Author contributions

J.X. and J.L. developed the original idea and designed the study. J.L., J.Y., C.T., B.M., and J.X. wrote and revised the manuscript. J.L. and H.D. performed the experimental studies. J.L. and J.X. carried out the data analysis.

Competing interests

The authors declare no competing interests.

Additional information

Supplementary information The online version contains supplementary material available at https://doi.org/10.1038/s41467-024-54392-x.

Correspondence and requests for materials should be addressed to Jianming Xu.

Peer review information *Nature Communications* thanks Chao Ai, Wei-Min Sun and the other anonymous reviewer(s) for their contribution to the peer review of this work. A peer review file is available.